Accepted Article

Title: f-block MOFs: A Pathway to Heterometallic Transuranics

Authors: Kyoung Chul Park, Preecha Kittikhunnatham, Jaewoong Lim, Grace C. Thaggard, Yuan Liu, Corey R. Martin, Gabrielle A. Leith, Donald J. Toler, An T. Ta, Nancy Birkner, Ingrid Lehman-Andino, Alejandra Hernandez-Jimenez, Gregory Morrison, Jake W. Amoroso, Hans-Conrad zur Loye, Dave P. DiPrete, Mark D. Smith, Kyle S. Brinkman, Simon R. Phillpot, and Natalia B. Shustova

WILEY-VCH

RESEARCH ARTICLE

f-block MOFs: A Pathway to Heterometallic Transuranics

Kyoung Chul Park,[a] Preecha Kittikhunnatham,[b] Jaewoong Lim,[a] Grace C. Thaggard,[a] Yuan Liu,[c] Corey R. Martin,[d] Gabrielle A. Leith,[a] Donald J. Toler,[a] An T. Ta,[c] Nancy Birkner,[e],[f] Ingrid Lehman-Andino,[d] Alejandra Hernandez-Jimenez,[d] Gregory Morrison,[a] Jake W. Amoroso,[d] Hans-Conrad zur Loye,[a],[d] Dave P. DiPrete,[d] Mark D. Smith,[a] Kyle S. Brinkman,[e],[f] Simon R. Phillpot,[c] and Natalia B. Shustova*[a]

[a] K. C. Park, Dr. J. Lim, G. C. Thaggard, Dr. G. A. Leith, D. J. Toler, Dr. G. Morrison, Prof. Dr. H.-C. zur Loye, Dr. M. D. Smith, Prof. Dr. N. B. Shustova
Department of Chemistry and Biochemistry
University of South Carolina
Columbia, SC 29208 (USA)
E-mail: shustova@sc.edu
[b] Prof. Dr. P. Kittikhunnatham
Department of Chemistry
Chulalongkorn University
Bangkok, 10330 (Thailand)
[c] Y. Liu, Dr. A. T. Ta, Prof. Dr. S. R. Phillpot
Department of Materials Science and Engineering
University of Florida
Gainesville, FL 32611 (USA)
[d] Dr. C. R. Martin, Dr. I. Lehman-Andino, Dr. A. Hernandez-Jimenez, Dr. J. W. Amoroso, Prof. Dr. H.-C. zur Loye, Dr. D. P. DiPrete
Savannah River National Laboratory
Aiken, SC 29808 (USA)
[e] Dr. N. Birkner, Prof. Dr. K. S. Brinkman
Department of Materials Science and Engineering
Clemson University
Clemson, SC 29634 (USA)
[f] Dr. N. Birkner, Prof. Dr. K. S. Brinkman
Center for Nuclear Environmental Engineering Sciences and Radioactive Waste Management (NEESRWM)
Clemson University
Clemson, SC 29634 (USA)

Supporting information for this article is given via a link at the end of the document.

Abstract: A novel series of heterometallic *f*-block-frameworks including the first examples of transuranic heterometallic ^{238}U/^{239}Pu-metal-organic frameworks (MOFs) and a novel monometallic ^{239}Pu-analog are reported. In combination with theoretical calculations, we probed the kinetics and thermodynamics of heterometallic actinide(An)-MOF formation and reported the first value of a U-to-Th transmetallation rate. We concluded that formation of uranyl species could be a driving force for solid-state metathesis. Density of states near the Fermi edge, enthalpy of formation, band gap, proton affinity, and thermal/chemical stability were probed as a function of metal ratios. Furthermore, we achieved 97% of the theoretical maximum capacity for An-integration. These studies shed light on fundamental aspects of actinide chemistry and also foreshadow avenues for the development of emerging classes of An-containing materials, including radioisotope thermoelectric generators or metalloradiopharmaceuticals.

Introduction

Both fundamental and industrial factors are driving forces for recent studies performed in an *f*-block-metal-organic frameworks (MOFs) sector. Applications of *f*-block MOFs as scintillators, hard radiation detectors, absorbers with a high selectivity toward specific actinides, or sensors for highly volatile radioactive species are the obvious directions in this area without taking into
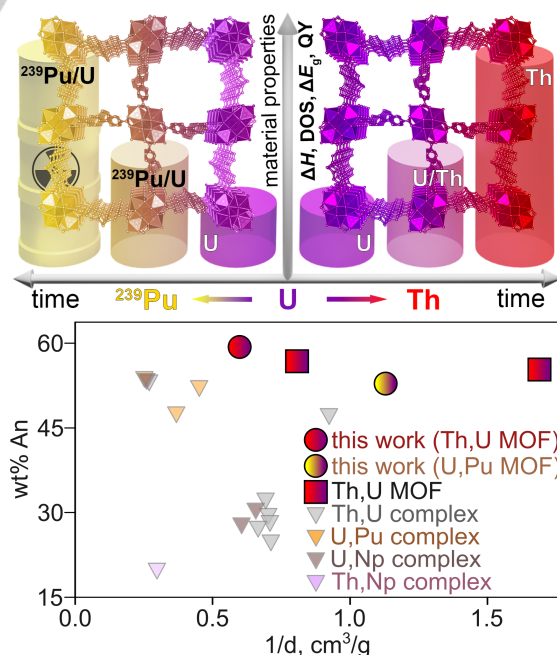
Scheme 1. (*top*) A schematic representation of changes in properties of heterometallic actinide-containing MOFs as a function of degree of transmetallation from U (purple) to Th (red) and Pu (yellow). (*bottom*) Calculated weight percent for all reported heterometallic An-MOFs and heterometallic An-molecular complexes as a function of structural 1/*d* (*d* = density).[1–11]

RESEARCH ARTICLE

account emerging classes of An-based materials for radioisotope thermoelectric generators or metalloradiopharmaceuticals.[12–40]

At the same time, fundamental aspects including relativistic effects through mixing of excited and ground states, *f*–*f* transitions in crystal fields, or pronounced spin-orbit coupling are cornerstones of inorganic, physical, and materials chemistry which could lead to coordination environments that are uncommon in transition metal systems, resulting in unique physicochemical properties or unusual structural motifs.[41–49] Another area which has not been explored yet is preparation of actinide-based frameworks containing actinides with mixed metal oxidation states.[50] Currently, reports on *f*-block MOFs, especially those containing transuranic elements, mainly focus on detailed structural analysis, while studies toward material properties have only very recently emerged (Scheme 1). As shown in Scheme 1, only four structures of heterometallic *f*-block MOFs have been reported[1,2,20,51] to date (including the two from this work) in contrast to over 1000 reports focused on *d*-element-based multimetallic frameworks, and therefore, there is not only a gap in studies of properties of heterometallic *f*-element-containing frameworks, but also in access to their synthetic routes. For instance, their preparation usually relies on successful crystal growth from a corresponding organic linker and metal salt, whereas the solid-state metathesis techniques successfully employed for *d*-block elements in MOFs[52,53] are nearly unexplored in *f*-block MOFs. Transmetallation in MOFs offers the advantage of preparing materials with already-known topology since a pre-synthesized MOF is utilized as a precursor, in contrast to a mixture of salts and linkers used in direct synthesis.[53–58]

Herein, we employ solid-state metathesis to prepare the first example of a heterometallic ^{238}U/^{239}Pu-MOF, as well as the first Pu-based framework isostructural to UiO-67. Furthermore, we report a trend in physicochemical properties of a series of heterometallic U/Th-containing frameworks as a function of metal ratio for the first time (Scheme 1). We employ a comprehensive analysis using theoretical modeling to correlate thermochemistry data with the observed trends, as well as to estimate density of states near the Fermi edge and corresponding band gaps in comparison with experimentally estimated values in the prepared heterometallic U/Th-frameworks. We also evaluated kinetics and thermodynamics of the U-to-Th process including a transmetallation rate for the first time and demonstrated that the formation of a very stable UO_2^{2+} moiety is a driving force that promotes the process of solid-state metathesis. Using theoretical analysis, we also shed light on the possibility of utilizing the uranium-containing MOF as a precursor to probe the preparation of heterometallic U/Pu-analogs. Furthermore, we explored the modularity of MOFs, including metal nodes, metal node extension, linkers, and pores to maximize actinide content within a single material, resulting in 97% actinide incorporation based on the theoretical maximum capacity.

Results and Discussion

In contrast to numerous studies focused on the preparation of actinide-containing frameworks from the corresponding salts and linkers, in the current work, we utilized the advances in the MOF field to employ actinide(An)-MOFs as reactants. The MOF selection was conducted based on the assumption that the presence of unsaturated metal nodes in the An-MOF structure

(i.e., with less than 12 organic linkers per node) could facilitate the second actinide integration through diminishing steric components, and that such nodes would be less stabilized by the coordination environment making them more susceptible to solid state metathesis. As a result, An-Me$_2$BPDC-8, An$_6$O$_4$(OH)$_8$(Me$_2$BPDC)$_4$, (An^{4+} = U^{4+}, Th^{4+}; Me$_2$BPDC^{2-} = 2,2′-dimethylbiphenyl-4,4′-dicarboxylate) possessing the *bcu*-topology, in which the organic linker is connected by eight-coordinated metal nodes, have been selected and synthesized (Figure 1; more detailed synthetic procedures can be found in the Supporting Information (SI)). Using the prepared An-Me$_2$BPDC-8 MOFs, we explored different pathways for the preparation of multiactinide heterometallic frameworks.
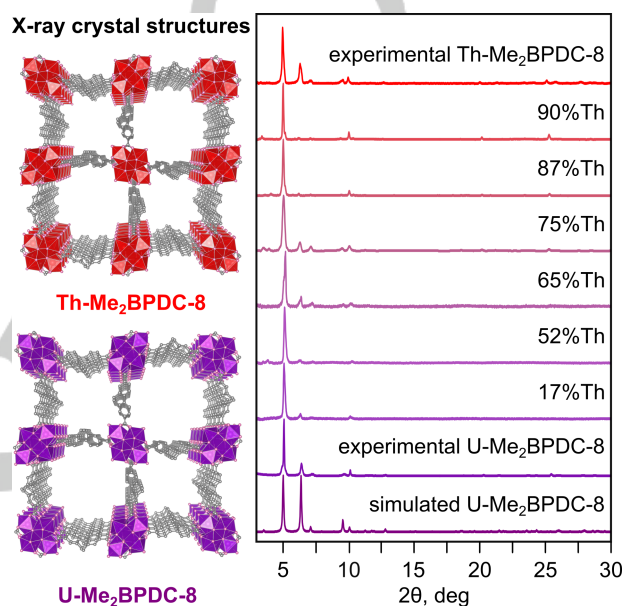

Figure 1. (*left*) Single-crystal X-ray structures of U- and Th-Me₂BPDC-8. (*right*) PXRD patterns of U/Th-Me₂BPDC-8 with various thorium content (%Th, the transition from purple to red colors represents the increase of the Th content).

Initially, we targeted different synthetic pathways for integration of multiple actinides with a detailed focus on thermodynamic and kinetic aspects of such processes and followed up with studies of the electronic structure and physicochemical properties of heterometallic An-MOFs. As a starting point, we have used U-Me₂BPDC-8 as a precursor to pursue solid-state metathesis using thorium nitrate as the Th source for preparation of heterometallic U/Th-containing analogs, while monitoring the actinide concentration and time as variables to control the degree of transmetallation. Our initial experiments provide an interesting insight, namely that the U→Th transmetallation could be switched on and off through alternation of experimental conditions. For instance, under anaerobic conditions the transmetallation did not occur even after several months (i.e., U-Me₂BPDC-8 stays intact in the presence of the thorium salt under an inert atmosphere using oxygen-free solvent), while transmetallation was rapidly completed in air. Interestingly, all attempts to use Th-MOFs as a precursor for uranium integration using the same method and experimental conditions were completely unsuccessful as confirmed by ICP-MS. In all cases, transmetallation occurred with preservation of the parent framework integrity as confirmed through PXRD analysis (Figure 1). Taking into account the experimental observations, we hypothesized that the formation of

2

RESEARCH ARTICLE

stable UO_2^{2+} could be a driving force for the successful U→Th transmetallation process, i.e., the replacement of U(IV) to Th(IV) is accompanied with oxidation of the former and formation of stable UO_2^{2+} species.
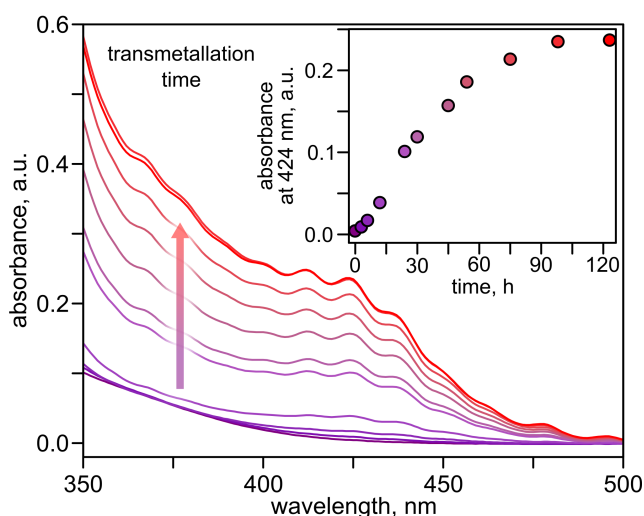

Figure 2. Time-dependent UV-vis spectra of the supernatant to monitor progress of the U→Th transmetallation reaction using a U-Me₂BPDC-8 as a precursor. The inset shows changes of supernatant absorbance at 424 nm as a function of transmetallation reaction time.

To test our hypothesis, we studied the kinetics and thermodynamics of the reported processes. In particular, we monitored the rate of the U→Th conversion spectrophotometrically through analysis of the supernatant solution. As shown in Figure 2, the intensity of the absorption bands at λ_{max} = 424 nm, associated with the UO_2^{2+} $\pi-\pi^*$ transitions,[59–61] increased over time, which is consistent with the increased concentration of UO_2^{2+} as transmetallation progresses. Moreover, the transmetallation progress could be estimated visually due to changes in the color of the supernatant from colorless to bright yellow. We estimated the corresponding rate constant by monitoring the appearance of UO_2^{2+} during the reaction progress. We hypothesized that the UO_2^{2+} release from the MOF matrix could be described as a first-order process, similar to our previous studies associated with radionuclide leaching from porous matrices.[39,62] In order to test our hypothesis, we fitted our experimental data using multiple theoretical models, such as zero-, first-, and second-order models, similar to studies of our group and others performed on different MOF systems.[39,62–66] Indeed, an analysis of the fittings based on evaluation of the goodness-of-fit parameter demonstrates that the transmetallation process could be described by a first-order rate model with the rate constant of uranyl formation k_1 = 5.64 × 10⁻⁶ s⁻¹. To the best of our knowledge, the reported rate constant is not only the first attempt to quantify the transmetallation process in An-MOFs, but it is the first rate constant value reported for the transmetallation process in MOFs in general. The determined rate constant is in agreement with values (same order of magnitude, double-exponential model fitting[62,66]) previously estimated for cation release from the framework pores.[62] The matching rate constant values allow us to anticipate that the observed process of uranyl formation during transmetallation is mainly associated with framework-to-solution diffusion of UO_2^{2+}.[62] We built this

conclusion based on our previous studies of UO_2^{2+} leaching kinetics from porous materials.[62] We found that in contrast to the leaching process of the pre-absorbed UO_2^{2+} cations,[62] which occurs via two steps (corresponding to an initial fast cation release from the framework surface followed by a slow, kinetically hindered release of cations from the bulk of the material[67]), kinetics of UO_2^{2+} formation due to transmetallation could be described as a one step process. Indeed, in the present studies, the UO_2^{2+} formation occurs in situ versus the previous report in which UO_2^{2+} was initially loaded into the framework by immersing the MOF into the UO_2^{2+} solution.
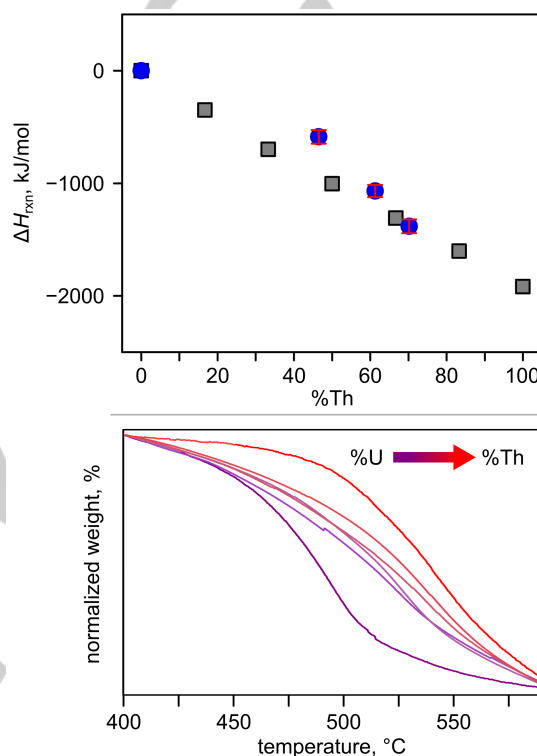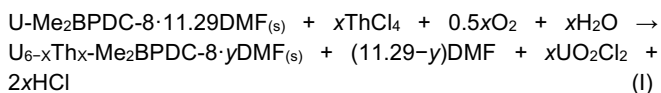

Figure 3. (*top*) Calculated $\Delta H^\circ_{rxn(calc)}$ (gray squares) and ΔH°_{rxn} (blue circles) for the U→Th transmetallation reaction as a function of %Th. Red bars represent the standard error of the average value. (*bottom*) TGA plots of evacuated U/Th-Me₂BPDC-8 with various %Th. The transition from purple to red colors of TGA plots correspond to 0%, 47%, 61%, 70%, 93%, and 100% of thorium in the metal nodes of U/Th-Me₂BPDC-8. The TGA data were normalized to 100% at 400 °C for better visualization of framework stability.

As expected, there are no surface-trapped uranyl species in the present studies due to the different mechanism of the transmetallation reaction, and therefore, the observed cation release has been described as a first-order process. As a next step, we evaluated the standard enthalpy of the transmetallation reaction, ΔH°_{rxn}, i.e., formation of heterometallic U/Th-Me₂BPDC-8. To estimate ΔH°_{rxn}, we first performed room temperature solution calorimetry measurements. Specifically, we determined the enthalpies of dissolution (ΔH°_{ds}) for monometallic U-Me₂BPDC-8 and heterometallic U/Th-Me₂BPDC-8 with a different %Th content as shown in Table 1. The enthalpy of formation for each An-Me₂BPDC-8 (ΔH°_f) was calculated from experimentally measured and related thermodynamic values given in Table 1 using thermochemical cycle reaction equations as explained in more details in the SI. Moreover, we further calculated the standard enthalpy of the transmetallation reaction,

3

WILEY-VCH

RESEARCH ARTICLE

ΔH°_{rxn}, for each U/Th-Me$_2$BPDC-8 by applying Eq. 1 to the transmetallation reaction carried out in the presence of oxygen (reaction I) using the appropriate standard enthalpies of formation of the reaction components (Tables 1, S1, and S2). The estimated values of ΔH°_{rxn} as a function of a degree of transmetallation are shown in Figure 3.

$$\Delta H^{\circ}_{rxn} = \Sigma a \Delta H^{\circ}_f \text{ (products)} - \Sigma b \Delta H^{\circ}_f \text{ (reactants)} \qquad \text{(Eq. 1)}$$

U-Me$_2$BPDC-8·11.29DMF$_{(s)}$ + xThCl$_4$ + 0.5xO$_2$ + xH$_2$O → U$_{6-x}$Th$_x$-Me$_2$BPDC-8·yDMF$_{(s)}$ + (11.29−y)DMF + xUO$_2$Cl$_2$ + 2xHCl   (I)

Based on the analysis of the thermochemical studies, the higher degree of %Th content incorporated into the U-Me$_2$BPDC-8 resulted in more negative values of ΔH°_{rxn}, suggesting that the U→Th transmetallation reaction is exothermic. In contrast, the reaction
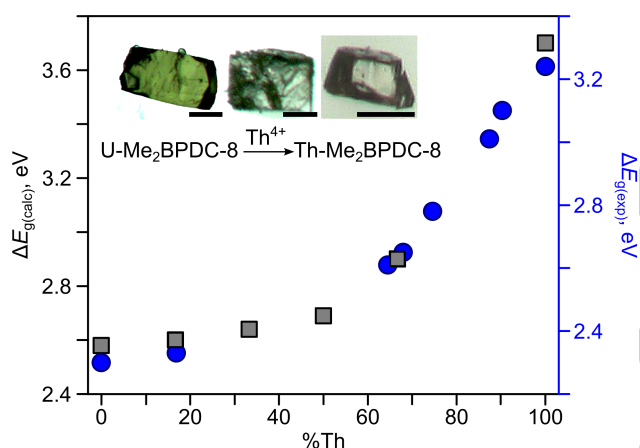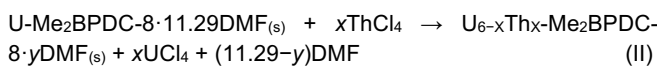
U-Me$_2$BPDC-8·11.29DMF$_{(s)}$ + xThCl$_4$ → U$_{6-x}$Th$_x$-Me$_2$BPDC-8·yDMF$_{(s)}$ + xUCl$_4$ + (11.29−y)DMF   (II)

Figure 4. Calculated (gray squares) and experimental optical band gaps (blue circles) of U/Th-Me$_2$BPDC-8 as a function of %Th. The insets show optical micrographs of U/Th-Me$_2$BPDC-8 with different levels of Th substitution. The scale bars are 20 μm.

in which transmetallation occurs without changes in the uranium oxidation state (i.e., U^{+4} after the replacement by Th^{+4} remains in the +4 oxidation state (reaction II)) is energetically less favorable. For instance, ΔH°_{rxn} of the reaction that converts U-Me$_2$BPDC-8 metal nodes to U$_{3.2}$Th$_{2.8}$-Me$_2$BPDC-8 ones using Eq.1 (reaction II) was estimated to be +176.79 kJ/mol versus −587.57 kJ/mol estimated using Eq.1 (reaction I), where the latter was calculated for the reaction associated with the formation of a uranyl species. These studies also shed light on the experimental outcome of the unsuccessful reverse Th→U transformations. Thus, these values are in line with our observations and the hypothesis that the formation of stable uranyl species through U(IV) oxidation could be the driving force for transmetallation to occur. Moreover, they uncover a useful synthon, U-Me$_2$BPDC-8, for incorporation of other radionuclides as discussed below. To further support our experimental findings, we also performed theoretical calculations to determine the calculated enthalpy of transmetallation reaction. Specifically, we calculated $\Delta H^{\circ}_{rxn(calc)}$ for U→Th substitution using

density functional theory (DFT) on the truncated models, U$_{6-x}$Th$_x$(HCO$_2$)$_8$O$_8$ (x = 0–6) as shown in Figure 6. The DFT-calculated values of $\Delta H^{\circ}_{rxn(calc)}$ agreed with the experimentally determined trend (Figure 3), demonstrating that the larger degree of transmetallation with Th results in larger negative values of calculated $\Delta H^{\circ}_{rxn(calc)}$. Thus, the calculated enthalpy of transmetallation reaction indicates that U→Th substitution is an energetically favorable process.

Table 1. Enthalpies of formation of U/Th-Me$_2$BPDC-8 and H$_2$Me$_2$BPDC calculated from experimental thermodynamic data.[a]

	ΔH°_{ds}, kJ/mol	ΔH°_f, kJ/mol
U-Me$_2$BPDC-8	−221[b] ± 27	−12986[c] ± 42
U$_{3.2}$Th$_{2.8}$-Me$_2$BPDC-8	−419[b] ± 38	−13101[c] ± 44
U$_{2.3}$Th$_{3.7}$-Me$_2$BPDC-8	−274[b] ± 32	−15568[c] ± 42
U$_{1.8}$Th$_{4.2}$-Me$_2$BPDC-8	−105[b] ± 42	−15925[c] ± 50
H$_2$Me$_2$BPDC	4.48[20] ± 0.06	−715.2[20] ± 1.0
DMF	−9.45[20] ± 0.01	−239.4[20] ± 1.2
ThCl$_4$	−250.4[c] ± 2.6	−1186.3[68] ± 1.3
UO$_2$Cl$_2$	−109.4[c] ± 2.0	−1243.6[69] ± 1.3
HCl	0	−166.99[70] ± 0.02
H$_2$O	0	−285.83[20] ± 0.1

[a] ΔH°_{ds} (*left*) and ΔH°_f (*right*) are the enthalpies of dissolution and formation, respectively.

[b] Average of the measurements.

[c] Detailed information can be found in the SI.

We also performed thermal stability studies via thermogravimetric analysis (TGA) and found that the thermal stability is in line with the described thermodynamics data. The TGA plots show a stepwise weight loss upon heating of the monometallic and heterometallic MOFs under a nitrogen atmosphere (Figure S3). The first step in the TGA curves (< 300 °C) is associated with the removal of the solvent, such as DMF, while the second step (> 350 °C) is associated with framework degradation (mainly due to the presence of organic linkers (Figures 3 and S3)).

According to the analysis of the acquired TGA results, the increase of the Th content in the U/Th-Me$_2$BPDC-8 shifts the MOF decomposition to a higher temperature range, demonstrating that thorium-containing MOFs have higher thermal stability as shown in Figure 3. During transmetallation experiments, we also noticed that the U→Th transmetallation process is accompanied by a drastic color change from dark green (U-Me$_2$BPDC-8) to colorless (Th-Me$_2$BPDC-8, Figure 4). We also explored the photoluminescence behavior of An-Me$_2$BPDC-8 (An^{4+} = U^{4+}, Th^{4+}) and detected a hypsochromic shift in emission upon increasing the thorium content as shown in Figure 5. For instance, λ_{max} was shifted from 513 to 497 nm when the Th content increased from 65% to 75%. In addition, epifluorescence microscopic images (Figure 5) displayed the same trend: a change in emission color of U/Th-Me$_2$BPDC-8 from green to blue with an increased thorium percentage (%Th). The increase of %Th also resulted in a slight enhancement of its photoluminescence quantum yields as shown in Figure 5. The changes in material color and photoluminescence

4

RESEARCH ARTICLE

properties provoked an investigation of changes in the U/Th-Me₂BPDC-8 electronic properties as a function of degree of transmetallation using diffuse reflectance (DR) spectroscopy and Tauc plot analysis with support from theoretical calculations. DR spectroscopic studies demonstrated a hypsochromic shift upon U→Th transmetallation which is associated with the trend of changes in the band gap estimated from the Tauc plot analysis (Figure S6). Indeed, the optical bandgap, $\Delta E_{g(exp)}$, increases from 2.30 eV (U-Me₂BPDC-8) to 3.24 eV (Th-Me₂BPDC-8), which is in line with the observed changes in An-MOF color upon the transmetallation process (Table S9).
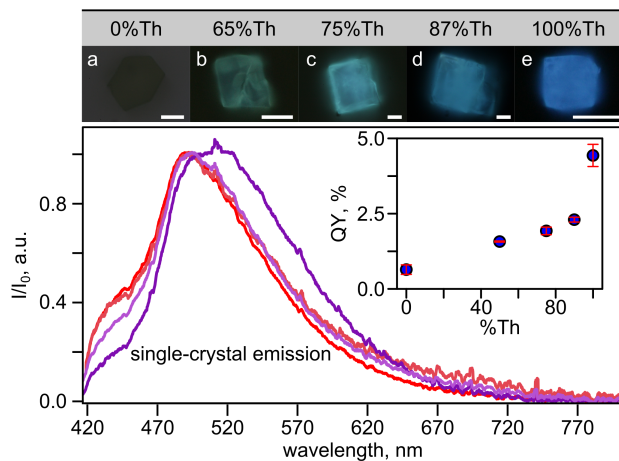

Figure 5. (*top*) Optical microscopic images of U/Th-Me₂BPDC-8 crystals with different metal ratios, collected in an epifluorescence mode. (*bottom*) Emission spectra of U/Th-Me₂BPDC-8 (λ_{ex} = 330–385 nm). The transition from purple to red represents 65%, 75%, 87%, and 100% of thorium in the metal nodes of U/Th-Me₂BPDC-8. The inset shows fluorescence quantum yields of U/Th-Me₂BPDC-8 with various %Th.

To shed light on the origin of such changes in the electronic structure, we performed *ab initio* band calculations with the plane wave basis set (Figure S1). The total and partial density of states (DOS) obtained from the lowest-energy configuration of each U/Th-Me₂BPDC-8 system (Figure 6) allowed for monitoring the changes in the DOS near the Fermi edge upon exchanging U⁴⁺ with Th⁴⁺ cations, using U-Me₂BPDC-8 as a precursor. The partial DOS shown in Figure 6 were obtained by adding the atomic projected DOS over different groups of elements, such as O, Th, and U. In the case of U₆-, U₅Th₁-, U₄Th₂-, U₃Th₃-, and U₂Th₄-models (Figure 6), the orbital-projected DOS suggest that DOS above E_F (conduction band) are dominated by U(5f) states with some degree of hybridization from O(2p) orbitals, while the DOS below E_F (valence band) are dominated by only U(5f) states. In contrast, for the Th₆ model, DOS above E_F (conduction band) are found to be dominated by O(2p) with very poor hybridization with the Th(5f) orbital, while DOS below E_F (valence band) are dominated by hybrid Th and O(2p) orbitals. Furthermore, we performed the calculations on one or more spin configurations for each truncated model (see the SI for more details). The band gap value of the U-containing SBU is dependent on the electrons' spin-polarization according to a literature report.[71] In Figure 4, the estimated band gap values ($\Delta E_{g(calc)}$) are shown which were evaluated through a weighted average of the band gap values obtained from all spin configurations (see SI for more details).

As a result, the estimated trend for $\Delta E_{g(calc)}$ values, which increase from 2.58 eV (U-Me₂BPDC-8) over the range of 2.60 eV (17%Th), 2.64 eV (33%Th), 2.69 eV (50%Th), 2.90 eV (67%Th), and 2.92 eV (83%Th) to 3.70 eV (Th-Me₂BPDC-8). They are also line with the ones determined for $\Delta E_{g(exp)}$ as shown in Figure 4 and Table S9. Interestingly, integration of the second actinide within the An-metal node also affects the proton affinity (i.e., enthalpy difference between the corresponding neutral and deprotonated states).
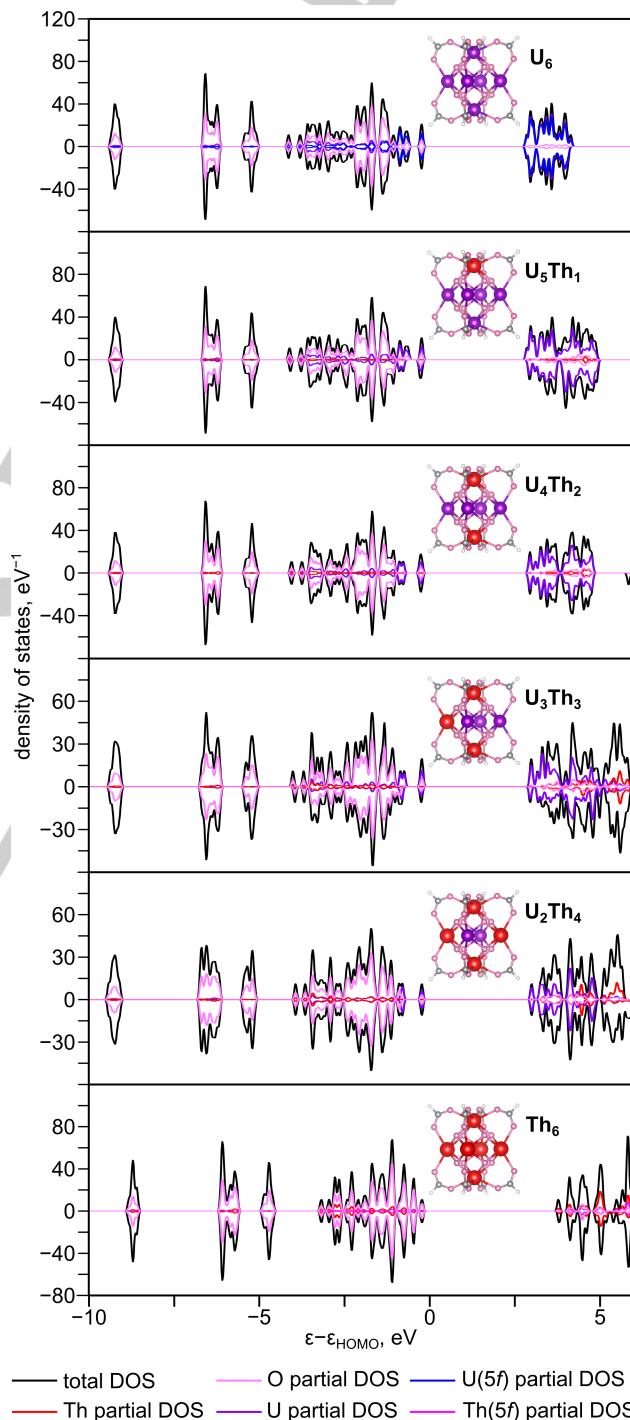

Figure 6. Partial and total DOS for U/Th-Me₂BPDC-8 with different U to Th ratios calculated from lowest-energy configurations. The insets show the truncated models of U/Th-Me₂BPDC-8 used for the DOS estimation.

5

WILEY-VCH

RESEARCH ARTICLE

As shown in Figure 7, there are three types of protons associated with the metal nodes of selected An-Me$_2$BPDC-8: terminal −OH$_2$ (H1, Figure 7) and terminal −OH (H2) as well as bridging −μ_3−OH (H3). DFT calculations revealed that affinities for H1 (324.0 kcal/mol), H2 (325.4 kcal/mol), H3 (327.1 kcal/mol) are smaller in the case of U-Me$_2$BPDC-8 in comparison with those estimated for Th-based nodes (330.0, 330.0, and 329.2 kcal/mol, respectively, Figure 7). Remarkably, overall there are only about eight examples[72–79] of such studies performed for heterometallic nodes including d-block MOFs despite the fact that this difference can be utilized for tailoring proton conductivity as shown in the example of heterometallic Zr/Ce MOFs.[79]
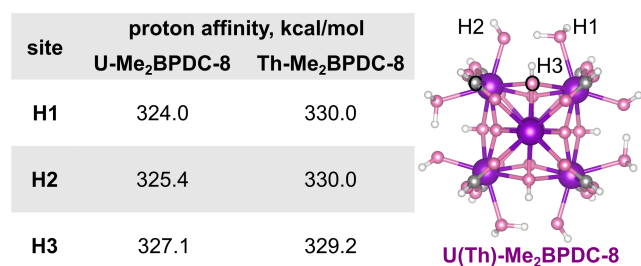
site	proton affinity, kcal/mol	
	U-Me$_2$BPDC-8	Th-Me$_2$BPDC-8
H1	324.0	330.0
H2	325.4	330.0
H3	327.1	329.2

Figure 7. Truncated model of U/Th-Me$_2$BPDC-8 nodes. Proton affinities were calculated for the protons of aquo groups (terminal −OH$_2$, H1), hydroxo groups (terminal −OH, H2), and bridging groups (bridging μ_3−OH, H3). The purple, pink, gray, and white spheres represent uranium (thorium), oxygen, carbon, and hydrogen atoms, respectively.
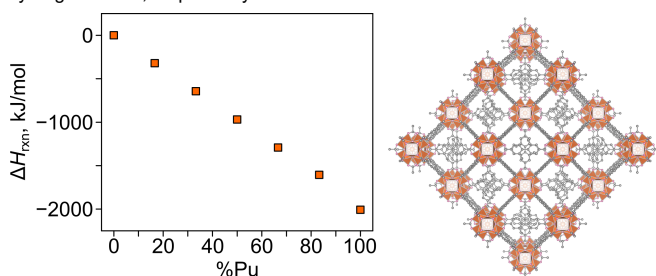

Figure 8. (*left*) Calculated $\Delta H°_{rxn(calc)}$ (orange squares) for the U^{4+}→Pu^{4+} transmetallation reaction as a function of %Pu. (*right*) Single-crystal X-ray structure of ^{239}Pu-Me$_2$BPDC-12. The orange, pink, and gray represent plutonium, oxygen, and carbon atoms, respectively. Hydrogen atoms were omitted for clarity.

As a proof of principle, we also tested the possibility of using U-Me$_2$BPDC-8 as a precursor for the incorporation of ^{239}Pu (6.2 × 10$^{−2}$ Ci/g), which is about 100,000 times more radioactive in comparison with the used ^{232}Th (1.1 × 10$^{−7}$ Ci/g) or ^{238}U (3.3 × 10$^{−7}$ Ci/g). The latter fact as well as safety restrictions placed on this work by Savannah River National Laboratory regulations dominated the choice of experimental conditions and the scope of work. As a source of ^{239}Pu, we used Pu(IV) nitrate which was loaded into U-Me$_2$BPDC-8 through its immersion into a DMF solution of ^{239}Pu(NO$_3$)$_4$ (1.00 × 10^5 Bq/mL). After three hours of U→^{239}Pu transmetallation, the resulting U/Pu-Me$_2$BPDC-8 samples were thoroughly rinsed and soaked in DMF to remove any residual plutonium salt. According to gamma-ray spectroscopic analysis, we were able to integrate about 0.1% of ^{239}Pu into our scaffold. Therefore, we increased the plutonium concentration by 82 times (8.20 × 10^6 Bq/mL) to enhance the degree of transmetallation. Indeed, after three and six hours of U^{4+}→^{239}Pu^{4+} transmetallation, the concentration of incorporated ^{239}Pu was increased by 10 times and 15 times, respectively.

Despite a relatively low ^{239}Pu loading, within several percent, the experiments were performed several times to confirm the extent of ^{239}Pu incorporation. In all cases, the performed structural analysis using PXRD confirmed structural integrity of the framework, and therefore, these studies are a first step to outline the possibility for incorporation of highly radioactive isotopes such as ^{239}Pu into a framework through solid-state metathesis (Figure S7).
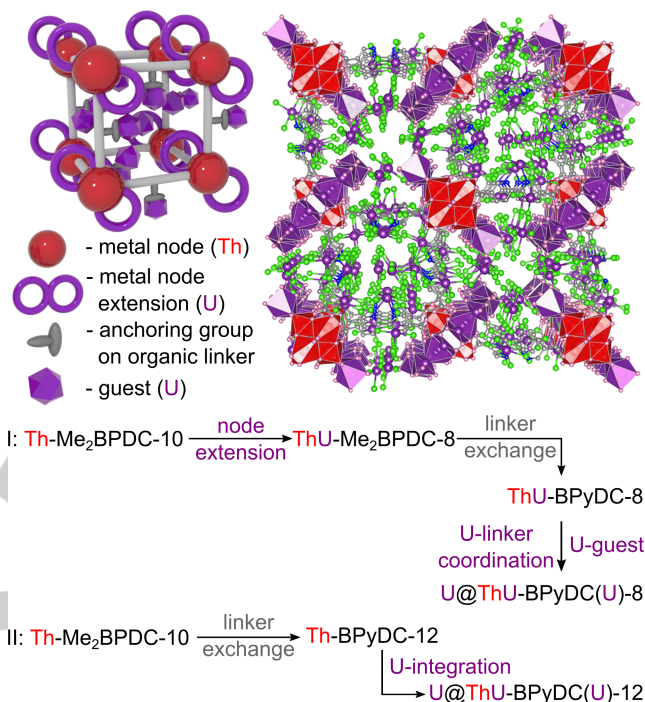
Scheme 2. (*top left*) Schematic representation of a heterometallic actinide MOF demonstrating different sites for uranium (purple) integration: as a part of the metal node through metal node extension, coordination to the organic linker, and as guest molecules. (*top right*) Model structure of U@ThU-BPyDC(U)-8. The red, purple, pink, gray, blue, and green spheres represent thorium, uranium, oxygen, carbon, nitrogen, and chlorine atoms, respectively. Hydrogen atoms were omitted for clarity. (*bottom*) Two pathways for actinide loading in MOFs.

More detailed studies regarding the rate of transmetallation, long-term framework stability upon ^{239}Pu integration, as well as probing the effects of increasing the degree of transmetallation are underway. Calculations of the enthalpy of transmetallation were performed in a similar way as described for U/Pu-Me$_2$BPDC-8. As shown in Figure 8, the DFT-calculated values of $\Delta H°_{rxn(calc)}$ demonstrate that the larger degree of transmetallation with Pu results in larger negative values of $\Delta H°_{rxn(calc)}$. Thus, the calculated enthalpy of the transmetallation reaction indicates that the U^{4+}→^{239}Pu^{4+} substitution is a favorable process. Interestingly, our attempts to prepare ^{239}Pu-Me$_2$BPDC-8 isostructural to U-Me$_2$BPDC-8 or Th-Me$_2$BPDC-8 using the direct synthesis were unsuccessful. Instead, we prepared ^{239}Pu-Me$_2$BPDC-12 isostructural to the UiO-67 analog using the direct method.[80] The PXRD pattern and ^{239}Pu-Me$_2$BPDC-12 metal node structures obtained through single-crystal X-ray studies are shown in Figure 8. Finally, we concluded our studies by testing the possibility to maximize actinide content through the utilization of multiple pathways for actinide integration such as in the metal node, metal node extension, linker coordination, and An-guest inclusion to prepare highly-loaded heterometallic An-frameworks with minimal

6

RESEARCH ARTICLE

$1/d$ (d = density, Scheme 1). We used two multistep approaches to achieve this goal as shown in Scheme 2. Approach **I** includes the following four steps: (1) synthesis of An-MOF, (2) metal node extension using UO_2^{2+},[1] (3) linker exchange to install 2,2′-bipyridine-5,5′-dicarboxylate ($BPyDC^{2-}$) possessing sites for actinide coordination, and (4) inclusion of An as guests. Approach **II** contains three steps: (1) the synthesis of An-MOF, (2) linker exchange to integrate $BPyDC^{2-}$, and (3) finally, An-inclusion as guests (see more details in the SI). The MOF selection was based on two criteria: presence of unsaturated metal nodes (i.e., containing less than 12 linkers per node) to promote metal node extension and (ii) chemical stability to undergo postsynthetic modifications such as linker exchange and metal node extension. As a result, we have chosen the thorium-based MOF, Th-Me$_2$BPDC-10, with 10-coordinated metal nodes as shown in Figure S14. The postsynthetic modification was carried out in the presence of uranyl acetate as a source of uranium to promote metal node extension. The actinide content in the prepared heterometallic An-MOFs was determined using ICP-MS, and the linker exchange was confirmed through ^1H NMR spectroscopy of the digested (destroyed in the presence of acid) MOF samples. Time, temperature, and actinide concentration were used as variables to maximize the actinide content. As a result, the maximum actinide content was achieved through approach **I**, and the maximum wt% was estimated as 60 wt% based on ICP-MS data, resulting in the highest reported content in heterometallic actinide-based frameworks at minimal reciprocal structural density, $1/d$ (d = density calculated from crystallographic data). Modeling of the theoretical maximum for actinide loading, taking into account the pore geometry, actinide-organic ligand chelating motif, as well as metal nodes and metal-node extension, resulted in 62 wt% maximum capacity, and therefore, we achieved 97% of the theoretical maximum.

Conclusion

To conclude, the first examples of heterometallic U/Pu MOFs and a monometallic Pu-MOF isostructural to UiO-67 have been prepared. Physicochemical properties of a novel series of U/Th-MOFs were explored as a function of a U:Th metal ratio, demonstrating increased thermo- and chemical stability in frameworks with a higher degree of Th incorporation. DOS near the Fermi edge and corresponding changes in the material band gaps were also studied upon enhancement of the Th content during the transmetallation process. In combination with the theoretical calculations, we probed kinetics and thermodynamics of heterometallic An-MOF formation, including the first reported value of a U-to-Th transmetallation rate. Based on the analysis of thermochemical studies, the higher degree of %Th content incorporated into U-MOFs resulted in more negative values of $\Delta H°_{rxn}$, suggesting that the U→Th transmetallation reaction is exothermic. We also established that one of the possible driving forces of the U-to-Th transmetallation is the formation of a stable uranyl species. The latter fact was supported by experimental and theoretical thermochemical data. A combination of strategies was also employed to maximize the actinide content within the same framework. For that, we used the Th-MOF containing $BPyDC^{2-}$ linkers with sites for actinide coordination, An-metal-node extension, and pore volume occupied by actinide cations. As a result, 97% of the theoretical maximum capacity has been achieved, leading to the material with the highest actinide wt% for the smallest reciprocal structural density, $1/d$. Overall, these studies highlight the potential for f-block MOFs to act as not only a platform for uncovering fundamental structure-property relationships, but also as precursors for well-defined transuranic-containing materials. As such, f-block MOFs could undoubtedly play a significant role in the development of upcoming radionuclide sequestration and repurposing methodologies that would alter the landscape of actinide research.

[1] E. A. Dolgopolova, O. A. Ejegbavwo, C. R. Martin, M. D. Smith, W. Setyawan, S. G. Karakalos, C. H. Henager, H.-C. zur Loye, N. B. Shustova, *J. Am. Chem. Soc.* **2017**, *139*, 16852–16861.

[2] Y. Wang, Y. Li, Z. Bai, C. Xiao, Z. Liu, W. Liu, L. Chen, W. He, J. Diwu, Z. Chai, T. E. Albrecht-Schmitt, S. Wang, *Dalton Trans.* **2015**, *44*, 18810–18814.

[3] A.-G. D. Nelson, T. H. Bray, F. A. Stanley, T. E. Albrecht-Schmitt, *Inorg. Chem.* **2009**, *48*, 4530–4535.

[4] G. T. Kent, X. Yu, C. Pauly, G. Wu, J. Autschbach, T. W. Hayton, *Inorg. Chem.* **2021**, *60*, 15413–15420.

[5] S. L. Staun, G. Wu, W. W. Lukens, T. W. Hayton, *Chem. Sci.* **2021**, *12*, 15519–15527.

[6] E. J. Schelter, R. Wu, B. L. Scott, J. D. Thompson, D. E. Morris, J. L. Kiplinger, *Angew. Chem. Int. Ed.* **2008**, *47*, 2993–2996; *Angew. Chem.* **2008**, *120*, 3035–3038.

[7] C. Tamain, B. A. Chapelet, M. Rivenet, F. Abraham, R. Caraballo, S. Grandjean, *Inorg. Chem.* **2013**, *52*, 4941–4949.

[8] A.-G. D. Nelson, T. H. Bray, T. E. Albrecht-Schmitt, *Angew. Chem. Int. Ed.* **2008**, *47*, 6252–6254; *Angew. Chem.* **2008**, *120*, 6348–6350.

[9] P. L. Arnold, M. S. Dutkiewicz, M. Zegke, O. Walter, C. Apostolidis, E. Hollis, A.-F. Pécharman, N. Magnani, J.-C. Griveau, E. Colineau, R. Caciuffo, X. Zhang, G. Schreckenbach, J. B. Love, *Angew. Chem. Int. Ed.* **2016**, *55*, 12797–12801; *Angew. Chem.* **2016**, *128*, 12989–12993.

7

RESEARCH ARTICLE

[10] I. A. Charushnikova, N. N. Krot, M. S. Grigor'ev, *Radiochemistry* **2014**, *56*, 468–475.

[11] J. Rebizant, C. Apostolidis, M. R. Spirlet, B. Kanellakopulos, *Inorganica Chim Acta* **1987**, *139*, 209–210.

[12] P. Li, N. A. Vermeulen, C. D. Malliakas, D. A. Gómez-Gualdrón, A. J. Howarth, B. L. Mehdi, A. Dohnalkova, N. D. Browning, M. O'Keeffe, O. K. Farha, *Science* **2017**, *356*, 624–627.

[13] Z. Chen, P. Li, X. Zhang, M. R. Mian, X. Wang, P. Li, Z. Liu, M. O'keeffe, J. F. Stoddart, O. K. Farha, *Nano Res.* **2021**, *14*, 376–380.

[14] P. Li, N. A. Vermeulen, X. Gong, C. D. Malliakas, J. F. Stoddart, J. T. Hupp, O. K. Farha, *Angew. Chem. Int. Ed.* **2016**, *55*, 10358–10362; *Angew. Chem.* **2016**, *128*, 10514–10518.

[15] S. L. Hanna, D. X. Rademacher, D. J. Hanson, T. Islamoglu, A. K. Olszewski, T. M. Nenoff, O. K. Farha, *Ind. Eng. Chem. Res.* **2020**, *59*, 7520–7526.

[16] S. E. Gilson, M. Fairley, P. Julien, A. G. Oliver, S. L. Hanna, G. Arntz, O. K. Farha, J. A. LaVerne, P. C. Burns, *J. Am. Chem. Soc.* **2020**, *142*, 13299–13304.

[17] L. J. Small, T. M. Nenoff, *ACS Appl. Mater. Interfaces* **2017**, *9*, 44649–44655.

[18] L. Cheng, C. Liang, W. Liu, Y. Wang, B. Chen, H. Zhang, Y. Wang, Z. Chai, S. Wang, *J. Am. Chem. Soc.* **2020**, *142*, 16218–16222.

[19] J. Li, B. Li, N. Shen, L. Chen, Q. Guo, L. Chen, L. He, X. Dai, Z. Chai, S. Wang, *ACS Cent. Sci.* **2021**, *7*, 1441–1450.

[20] O. A. Ejegbavwo, C. R. Martin, O. A. Olorunfemi, G. A. Leith, R. T. Ly, A. M. Rice, E. A. Dolgopolova, M. D. Smith, S. G. Karakalos, N. Birkner, B. A. Powell, S. Pandey, R. J. Koch, S. T. Misture, H.-C. zur Loye, S. R. Phillpot, K. S. Brinkman, N. B. Shustova, *J. Am. Chem. Soc.* **2019**, *141*, 11628–11640.

[21] B. Li, X. Dong, H. Wang, D. Ma, K. Tan, S. Jensen, B. J. Deibert, J. Butler, J. Cure, Z. Shi, T. Thonhauser, Y. J. Chabal, Y. Han, J. Li, *Nat. Commun.* **2017**, *8*, 485.

[22] B. Li, X. Dong, H. Wang, D. Ma, K. Tan, Z. Shi, Y. J. Chabal, Y. Han, J. Li, *Faraday Discuss.* **2017**, *201*, 47–61.

[23] L. Yang, M. Dincă, *Angew. Chem. Int. Ed.* **2021**, *60*, 23784–23789; *Angew. Chem.* **2021**, *133*, 23977–23982.

[24] H. Banda, J.-H. Dou, T. Chen, N. J. Libretto, M. Chaudhary, G. M. Bernard, J. T. Miller, V. K. Michaelis, M. Dincă, *J. Am. Chem. Soc.* **2021**, *143*, 2285–2292.

[25] J. Y. Choi, J. Flood, M. Stodolka, H. T. B. Pham, J. Park, *ACS Nano* **2022**, *16*, 3145–3151.

[26] S. M. Cohen, N. L. Rosi, *Inorg. Chem.* **2021**, *60*, 11703–11705.

[27] M. Kalaj, M. R. Momeni, K. C. Bentz, K. S. Barcus, J. M. Palomba, F. Paesani, S. M. Cohen, *Chem. Commun.* **2019**, *55*, 3481–3484.

[28] H. Yang, F. Peng, A. N. Hong, Y. Wang, X. Bu, P. Feng, *J. Am. Chem. Soc.* **2021**, *143*, 14470–14474.

[29] H. Yang, F. Peng, D. E. Schier, S. A. Markotic, X. Zhao, A. N. Hong, Y. Wang, P. Feng, X. Bu, *Angew. Chem. Int. Ed.* **2021**, *60*, 11148–11152; *Angew. Chem.* **2021**, *133*, 11248–11252.

[30] H. Yang, M. Luo, L. Luo, H. Wang, D. Hu, J. Lin, X. Wang, Y. Wang, S. Wang, X. Bu, P. Feng, T. Wu, *Chem. Mater.* **2016**, *28*, 8774–8780.

[31] M. Zhang, C. Liang, G.-D. Cheng, J. Chen, Y. Wang, L. He, L. Cheng, S. Gong, D. Zhang, J. Li, S.-X. Hu, J. Diwu, G. Wu, Y. Wang, Z. Chai, S. Wang, *Angew. Chem. Int. Ed.* **2021**, *60*, 9886–9890; *Angew. Chem.* **2021**, *133*, 9974–9978.

[32] R. Hardian, S. Dissegna, A. Ullrich, P. L. Llewellyn, M.-V. Coulet, R. A. Fischer, *Chem. Eur. J.* **2021**, *27*, 6804–6814.

[33] W. R. Heinz, I. Agirrezabal-Telleria, R. Junk, J. Berger, J. Wang, D. I. Sharapa, M. Gil-Calvo, I. Luz, M. Soukri, F. Studt, Y. Wang, C. Wöll, H. Bunzen, M. Drees, R. A. Fischer, *ACS Appl. Mater. Interfaces* **2020**, *12*, 40635–40647.

[34] K. D. Nguyen, C. Kutzscher, F. Drache, I. Senkovska, S. Kaskel, *Inorg. Chem.* **2018**, *57*, 1483–1489.

[35] B. Felsner, V. Bon, J. D. Evans, F. Schwotzer, R. Grünker, I. Senkovska, S. Kaskel, *Chem. Eur. J.* **2021**, *27*, 9708–9715.

[36] C. Michel, Y. Barré, L. De Windt, C. de Dieuleveult, E. Brackx, A. Grandjean, *J. Environ. Chem. Eng.* **2017**, *5*, 810–817.

[37] T. le Nedelec, A. Charlot, F. Calard, F. Cuer, A. Leydier, A. Grandjean, *New J. Chem.* **2018**, *42*, 14300–14307.

[38] V. Villemot, N. Dufour, S. Mauree, B. Sabot, G. H. V. Bertrand, M. Hamel, *Adv. Photonics Res.* **2022**, *3*, 2100259.

[39] K. C. Park, C. R. Martin, G. A. Leith, G. C. Thaggard, G. R. Wilson, B. J. Yarbrough, B. K. P. Maldeni Kankanamalage, P. Kittikhunnatham, A. Mathur, I. Jatoi, M. A. Manzi, J. Lim, I. Lehman-Andino, A. Hernandez-Jimenez, J. W. Amoroso, D. P. DiPrete, Y. Liu, J. Schaeperkoetter, S. T. Misture, S. R. Phillpot, S. Hu, Y. Li, A. Leydier, V. Proust, A. Grandjean, M. D. Smith, N. B. Shustova, *J. Am. Chem. Soc.* **2022**, *144*, 16139–16149.

[40] K. Lv, S. Fichter, M. Gu, J. März, M. Schmidt, *Coord. Chem. Rev.* **2021**, *446*, 214011.

[41] C. R. Martin, G. A. Leith, N. B. Shustova, *Chem. Sci.* **2021**, *12*, 7214–7230.

[42] E. A. Dolgopolova, A. M. Rice, N. B. Shustova, *Chem. Commun.* **2018**, *54*, 6472–6483.

[43] H.-C. zur Loye, T. Besmann, J. Amoroso, K. Brinkman, C. H. Henager, S. Hu, S. T. Misture, S. R. Phillpot, N. B. Shustova, H. Wang, R. J. Koch, G. Morrison, E. Dolgopolova, *Chem. Mater.* **2018**, *30*, 4475–4488.

[44] S. E. Gilson, P. Li, J. E. S. Szymanowski, J. White, D. Ray, L. Gagliardi, O. K. Farha, P. C. Burns, *J. Am. Chem. Soc.* **2019**, *141*, 11842–11846.

[45] S. E. Gilson, M. Fairley, S. L. Hanna, J. E. S. Szymanowski, P. Julien, Z. Chen, O. K. Farha, J. A. LaVerne, P. C. Burns, *J. Am. Chem. Soc.* **2021**, *143*, 17354–17359.

[46] L. S. Natrajan, *Coord. Chem. Rev.* **2012**, *256*, 1583–1603.

[47] B. G. Wybourne, L. Smentek, *J. Alloys. Compd.* **2002**, *341*, 71–75.

[48] P. Zhang, H. Liu, W. Zou, P. Zhang, S.-X. Hu, *J. Phys. Chem. A* **2020**, *124*, 8173–8183.

[49] K. Lv, C. Urbank, M. Patzschke, J. März, P. Kaden, S. Weiss, M. Schmidt, *J. Am. Chem. Soc.* **2022**, *144*, 2879–2884.

[50] J. Liu, L. R. Redfern, Y. Liao, T. Islamoglu, A. Atilgan, O. K. Farha, J. T. Hupp, *ACS Appl. Mater. Interfaces* **2019**, *11*, 47822–47829.

[51] C. R. Martin, G. A. Leith, P. Kittikhunnatham, K. C. Park, O. A. Ejegbavwo, A. Mathur, C. R. Callahan, S. L. Desmond, M. R. Keener, F. Ahmed, S. Pandey, M. D. Smith, S. R. Phillpot, A. B. Greytak, N. B. Shustova, *Angew. Chem. Int. Ed.* **2021**, *60*, 8072–8080; *Angew. Chem.* **2021**, *133*, 8152–8160.

[52] S. M. Cohen, *Chem. Rev.* **2012**, *112*, 970–1000.

[53] Y. Lee, S. Kim, J. K. Kang, S. M. Cohen, *Chem. Commun.* **2015**, *51*, 5735–5738.

[54] M. Lalonde, W. Bury, O. Karagiaridi, Z. Brown, J. T. Hupp, O. K. Farha, *J. Mater. Chem. A* **2013**, *1*, 5453–5468.

[55] J. Park, D. Feng, H.-C. Zhou, *J. Am. Chem. Soc.* **2015**, *137*, 11801–11809.

[56] C. K. Brozek, V. K. Michaelis, T.-C. Ong, L. Bellarosa, N. López, R. G. Griffin, M. Dincă, *ACS Cent. Sci.* **2015**, *1*, 252–260.

[57] A. W. Stubbs, L. Braglia, E. Borfecchia, R. J. Meyer, Y. Román-Leshkov, C. Lamberti, M. Dincă, *ACS Catal.* **2018**, *8*, 596–601.

[58] B. Garai, V. Bon, S. Krause, F. Schwotzer, M. Gerlach, I. Senkovska, S. Kaskel, *Chem. Mater.* **2020**, *32*, 889–896.

[59] X. Sun, C. Samples, K. Daia, M. Meyers, M. Bumgarner, *J. Chem. Res.* **2009**, 351–355.

[60] X. Sun, D. R. J. Kolling, H. Mazagri, B. Karawan, C. Pierron, *Inorganica Chim Acta* **2015**, *435*, 117–124.

[61] D. L. Clark, S. D. Conradson, R. J. Donohoe, D. W. Keogh, D. E. Morris, P. D. Palmer, R. D. Rogers, C. D. Tait, *Inorg. Chem.* **1999**, *38*, 1456–1466.

[62] A. A. Berseneva, C. R. Martin, V. A. Galitskiy, O. A. Ejegbavwo, G. A. Leith, R. T. Ly, A. M. Rice, E. A. Dolgopolova, M. D. Smith, H.-C. zur Loye, D. P. Diprete, J. W. Amoroso, N. B. Shustova, *Inorg. Chem.* **2020**, *59*, 179–183.

[63] Y. Zhang, K. P. Hart, W. L. Bourcier, R. A. Day, M. Colella, B. Thomas, Z. Aly, A. Jostsons, *J. Nucl. Mater.* **2001**, *289*, 254–262.

[64] C. G. Varelas, D. G. Dixon, C. A. Steiner, *J. Control. Release* **1995**, *34*, 185–192.

[65] F. Faraji, A. Alizadeh, F. Rashchi, N. Mostoufi, *Rev. Chem. Eng.* **2022**, *38*, 113–148.

[66] H. Huang, H. Sato, T. Aida, *J. Am. Chem. Soc.* **2017**, *139*, 8784–8787.

[67] M. N. Freitas, J. M. Marchetti, *Int. J. Pharm.* **2005**, *295*, 201–211.

RESEARCH ARTICLE

[68] M. Rand, J. Fuger, I. Grenthe, V. Neck, D. Rai, *Chemical Thermodynamics of Thorium in Chemical Thermodynamics*, OECD publishing, Paris, **2008**.

[69] R. Guillaumont, T. Fanghänel, V. Neck, J. Fuger, D. A. Palmer, I. Grenthe, M. H. Rand, *Update on the Chemical Thermodynamics of Uranium, Neptunium, Plutonium, Americium and Technetium in Chemical Thermodynamics*, OECD publishing, Paris, **2008**.

[70] B. Ruscic, D. H. Bross, Active Thermochemical Tables (ATcT) values based on ver. 1.122 of the Thermochemical Network, Argonne National Laboratory, **2016**.

[71] S. Pandey, B. Demaske, O. A. Ejegbavwo, A. A. Berseneva, W. Setyawan, N. B. Shustova, S. R. Phillpot, *Comput. Mater. Sci.* **2020**, *184*, 109903.

[72] H. Wang, Q. Wu, X. Ding, Z. Shao, W. Xu, Y. Zhao, Q. Xie, X. Meng, H. Hou, *Inorg. Chem.* **2020**, *59*, 8361–8368.

[73] H.-N. Wang, H.-X. Sun, Y.-M. Fu, X. Meng, Y.-H. Zou, Y.-O. He, R.-G. Yang, *Inorg. Chem. Front.* **2021**, *8*, 4062–4071.

[74] K.-I. Otake, K. Otsubo, K. Sugimoto, A. Fujiwara, H. Kitagawa, *Angew. Chem. Int. Ed.* **2016**, *55*, 6448–6451; *Angew. Chem.* **2016**, *128*, 6558–6561.

[75] H. ŌKawa, M. Sadakiyo, K. Otsubo, K. Yoneda, T. Yamada, M. Ohba, H. Kitagawa, *Inorg. Chem.* **2015**, *54*, 8529–8535.

[76] H. ŌKawa, M. Sadakiyo, T. Yamada, M. Maesato, M. Ohba, H. Kitagawa, *J. Am. Chem. Soc.* **2013**, *135*, 2256–2262.

[77] H. ŌKawa, A. Shigematsu, M. Sadakiyo, T. Miyagawa, K. Yoneda, M. Ohba, H. Kitagawa, *J. Am. Chem. Soc.* **2009**, *131*, 13516–13522.

[78] M. Sadakiyo, H. ŌKawa, A. Shigematsu, M. Ohba, T. Yamada, H. Kitagawa, *J. Am. Chem. Soc.* **2012**, *134*, 5472–5475.

[79] W. H. Ho, S.-C. Li, Y.-C. Wang, T.-E. Chang, Y.-T. Chiang, Y.-P. Li, C.-W. Kung, *ACS Appl. Mater. Interfaces* **2021**, *13*, 55358–55366.

[80] N. Ko, J. Hong, S. Sung, K. E. Cordova, H. J. Park, J. K. Yang, J. Kim, *Dalton Trans.* **2015**, *44*, 2047–2051.

[81] CCDC 2209989–2209991 contains the supplementary crystallographic data for this paper. These data can be obtained free of charge from The Cambridge Crystallographic Data Centre.

9

RESEARCH ARTICLE

Entry for the Table of Contents
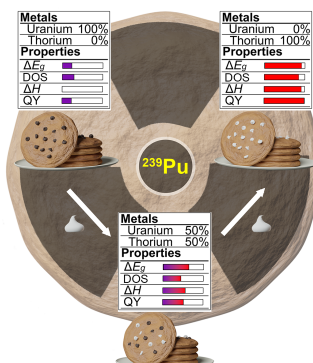
Like baking cookies to personal taste, preparation of a library of heterometallic actinide-MOFs allows for tailoring of the "flavor" of material properties. Mixing the radionuclide ingredients in proper ratios reveals structure-property relationships and unique design principles for new classes of actinide-based materials. In addition, the prepared frameworks provide a recipe for novel, pre-designed transuranic MOFs.

Institute and/or researcher Twitter usernames: ShustovaLab